A COMPARISON BETWEEN PULSED AND CW LASER ANNEALING FOR SOLAR CELL APPLICATIONS

G. E. Jellison, Jr., R. T. Young, and R. F. Wood
Oak Ridge National Laboratory*
Oak Ridge, Tennessee

and

A. Gat
Coherent Laser, Inc.
Palo Alto, California

ABSTRACT

It has been shown previously that pulsed laser annealing is an excellent technique for emitter fabrication in solar cells. Here it is shown that using shallow ^{75}As implantation (5 keV), plus the addition of a back-surface field and a gettering step, solar cell efficiencies of 16.6% have been obtained. Our initial attempts at fabrication of solar cells from CW laser-annealed material resulted in cells of inferior quality compared to cells fabricated using pulsed laser annealing techniques; this was because the CW laser annealing introduced recombination centers well into the base region of the cells.

INTRODUCTION

Over the last few years, it has been shown that pulsed laser annealing is an excellent technique for solar cell processing (refs. 1 and 2). Pulsed laser annealing is superior to conventional thermal annealing for 1) removal of lattice damage after ion implantation, 2) restoration of electrical activity, and 3) the preservation of the minority carrier diffusion length in the base region. It is widely believed that pulsed laser annealing involves the melting of the front damaged layer, followed by epitaxial regrowth from the perfect single crystal substrate. The resultant dopant profiles are usually considerably broadened from the preannealed condition; this broadening is readily explained by the melting model (see ref. 3). In addition to laser annealing of ion-implanted material, two other laser-assisted junction formation techniques have been employed: 1) laser-induced diffusion of deposited dopant films, and 2) laser-induced recrystallization of doped amorphous films (see ref. 1).

*Operated by Union Carbide Corporation for the U.S. Department of Energy under contract W-7405-eng-26.

Continuous wave (CW) laser annealing has also been useful for the annealing of ion-implanted emitter regions (ref. 4). However, CW laser annealing apparently takes place via a solid-phase recrystallization process, which does not change the initial dopant profile appreciably (ref. 5). This allows one to obtain extremely shallow junctions (< 200 nm), but results in a Gaussian emitter profile, which is less than optimum for solar cell applications, and also introduces several deep-lying defect states which can act as recombination centers (ref. 6).

This paper presents the latest results of our studies of the use of laser processing in solar cell fabrication. In particular, we will present a process developed at Oak Ridge National Laboratory for the fabrication of a 16.6% silicon solar cell using pulsed laser processing. Also, we will present results comparing pulsed laser annealing with CW laser annealing in solar cell fabrication.

HIGH EFFICIENCY SOLAR CELLS FROM PULSED LASER PROCESSING

Table 1 outlines the process that we have used for the fabrication of high efficiency silicon solar cells using pulsed laser processing on 10 Ω-cm substrates. The first step is ion-implantation using 5 keV As (n-on-p cells) or 5 keV B (p-on-n cells). This step results in a Gaussian impurity distribution profile with peaks < 20 nm deep; however, the front surface is either highly damaged (for the case of B) or amorphous (for the case of As), and the impurities are not fully electrically active. The laser annealing (step 3) is performed in air with a Q-switched ruby laser (λ = 694 nm, pulse width 15 ns) and with the substrate heated to 400°C. This results in nearly perfect recrystallization of the emitter region. The back side gettering (step 4) is performed to enhance the base minority carrier diffusion length. A high energy laser pulse (2.2-2.5 J/cm^2) is passed through a rough ground glass diffuser plate to homogenize the beam before it impinges on the sample. This pulse results in random but evenly distributed surface damage and introduces a high density of dislocations. The sample is then heated in an oxygen atmosphere at 1000°C for 1 h; this gettering step improves the minority carrier diffusion length from 100 μm to 400 μm in the best cases. The back-surface field (step 6) is then fabricated by the deposition of 10 nm of B or Sb followed by laser irradiation with a 1.8 J/cm^2 pulse. Fabrication of the finished cell is then completed by steps 7-10.

Our progress in the fabrication of solar cells using laser annealing techniques is outlined in Table 2. With just As implantation followed by laser annealing, cells with efficiencies up to 15.1% have been obtained (all solar cell parameters quoted were measured using a calibrated AM1 solar cell simulator). The total cell area is $\sim$ 2 cm^2); if a back-surface field is added by laser-induced diffusion, cells with efficiencies up to 16.1% can be obtained. The addition of the gettering step (steps 4 and 5) results in efficiencies of 16.6% and an open circuit voltage of 605 mV.

It should be noted that we use a single-layer Ta_2O_5 antireflection coating and no special solar cell geometries are employed. In spite of this, we

achieve very high cell efficiencies. For these reasons, we believe that laser techniques will prove to be extremely useful for the manufacture of high-efficiency solar cells.

COMPARISON OF PULSED AND CW LASER PROCESSING TECHNIQUES

Solar cells were fabricated from p-type substrates (10 Ω-cm), ion-implanted with As at 100 keV, and CW laser annealed using an argon-ion laser. The laser power was 11 watts, with a spot size of 100 μm, a scan rate of 25 cm/sec and a 50 μm lateral step after each scan. A back-surface field was fabricated by depositing B (10 nm) on the back of the cell and pulse laser annealing with a 1.8 J/cm^2 pulse (step 6 of Table 1). In addition to this procedure, some of the CW laser-annealed cells were subjected to a 700°C furnace anneal for 1 h. For comparison purposes, similar solar cells were fabricated using pulsed laser annealing techniques but with no gettering step (steps 1-3, 6-10 of Table 1). Three different implantation doses at 5 keV and one dose at 25 keV As implants were used. As mentioned above, CW laser annealing is a solid-phase epitaxial process that results in negligable dopant redistribution (refs. 4 and 5). Therefore, in order to get similar junction depths ($\sim$ 200 nm), a higher energy As implant had to be employed for the CW laser-annealed samples than for the pulsed laser-annealed samples. The resulting solar cell parameters are shown in Table 3. The results quoted for cells fabricated using pulsed laser annealing techniques were averaged over 2 to 4 cells, while the results quoted for the CW laser-annealed cells are for the best cells. Clearly, the pulsed laser-annealed cells perform better than the CW laser-annealed cells: both V_{oc} and J_{sc} are less in the CW laser-annealed samples, compared with the pulsed laser-annealed samples, though a 700°C furnace anneal for 1 h increases both V_{oc} and J_{sc} somewhat. Note also that V_{oc} is decreased in the pulse laser-annealed cells if the As acceleration voltage is increased from 5 keV to 25 keV, though J_{sc} remains constant.

A further comparison can be made by examining the spectral response (or quantum efficiency) data (shown in Fig. 1) for cells with no AR coating. As can be seen, the CW laser-annealed cells have a lower quantum efficiency than the pulsed laser-annealed cells at all wavelengths. A 700°C furnace anneal increases the quantum efficiency somewhat at all wavelengths, but this increase does not compare to the increase achieved using pulsed laser annealing. The poor blue response of the CW laser-annealed cells indicates very poor collection efficiency in the emitter region, while the poor red response is attributed to a low value of the minority carrier diffusion length in the base. Note that the CW laser-annealed cells were fabricated on different substrates than the pulsed laser-annealed samples, and the minority carrier diffusion length should not be expected to be the same.

Figure 2 a), b), and c) show the spectral response data for each individual cell, along with a calculated spectral efficiency. The calculated curve was obtained using a simple abrupt junction solar cell model with 9 parameters (H = cell thickness; W = depletion width, Xj = junction depth; Se, Sb = surface recombination velocity of the emitter and the base regions; Le, Lb = minority carrier diffusion length of the emitter and the base region; De, Db = the

diffusion coefficient of the emitter and the base regions.) Many of the parameters (H, W, Xj, De, Db) are known for each individual cell and were not varied, the absorption coefficient and reflectivity were taken from known data, and the back-surface field was modeled by setting Sb small (= 10^2 cm/sec), thus leaving 3 parameters to be determined (see Table 4) by minimizing the difference between the calculated and experimental points. The results of the modeling (shown in Fig. 2 and Table 4) indicate that: 1) It is necessary to eliminate the contribution of the emitter region of the CW laser-annealed cells in order to fit the blue response of these cells. 2) The minority carrier diffusion length required to fit the response of the CW laser-annealed cells was 100 μm (without furnace anneal) and 130 μm (with furnace anneal). 3) It was impossible to fit the data for the CW laser-annealed sample without post furnace anneal in the region from 0.5 to 0.85 μm using this simple model; this is possibly due to a layer of defects lying just below the depletion region (see the data described below) apparently produced by the CW laser annealing process.

Specific defects in CW laser-annealed material can be identified from DLTS (Deep Level Transient Spectroscopy) data. For the DLTS measurements, samples were prepared from the original solar cells by etching mesa diodes. One sample was fabricated by pulsed laser annealing a sample which had previously been CW laser annealed. Sample DLTS spectra are shown in Fig. 3 for the CW laser-annealed samples. No DLTS signal was observable from samples which had only been pulsed laser-annealed, and only a weak signal was observable in the CW laser-annealed sample after a 700°C furnace anneal. There are 3 traps observable: 2 (or more) electron (or minority carrier) traps, and 1 hole (or majority carrier trap).

The trap E-2 was observable only in the CW laser-annealed sample which had not also been pulsed laser annealed: Clearly the laser pulse annealed it out. Also, it has a broad spectrum, which indicates that it is in reality several traps. No further characterization of this trap was attempted.

The DLTS data for the traps E-1 and H-1 are presented in Table 5. Trap E-1 is a minority carrier trap close to the conduction band. It has a large minority carrier capture cross section, but once filled, a small majority carrier (or recombination) capture cross section. The pulsed laser annealing does not remove all of the E-1 traps, since the melt front produced by the ruby laser penetrates to a depth of less than 1 μm (ref. 3). By comparison, at a bias of -8V, the depletion regions of all our diodes extend to 4 μm beyond the junctions (the depletion region is the region of detectability in DLTS). Therefore, one would expect a maximum of $\sim$ 25% of the traps to be annealed out with the laser pulse, if the traps are evenly distributed throughout the depletion region. This is just what is observed. A trap with approximately this energy has been seen previously in CW laser-annealed samples (ref. 6), and in samples irradiated with electrons (ref. 7); it has been tentatively assigned to the familiar oxygen-vacancy complex, or A-center.

Trap H-1 is a majority carrier (or hole) trap, which lies closer to the conduction band than the valence band. It also is not removed by the pulsed laser-annealing process, but is removed by the furnace anneal. It has a majority carrier thermal capture cross section of 4×10^{-18} cm^2. To our knowledge, this trap has not been observed previously.

CW laser annealing has been shown to be useful for many semiconductor device fabrication applicatons; however, the data presented here shows that our best pulsed laser-annealed solar cells are better than solar cells we fabricated using the CW laser-annealing process. It was found that the CW laser-annealing process introduced a large number of recombination centers well into the bulk of the material, and that the emitter of CW laser-annealed solar cells was a very inefficient collector of minority carriers. However, it must be pointed out that this is our first attempt at fabricating solar cells from CW laser-annealed material and several improvements can be envisioned. For an ion implantation energy of 100 keV, the peak of the As profile is at 70 nm; therefore, the region from the surface to 70 nm will be ineffective for minority carrier collection, since the minority carriers will tend to be forced to the surface rather than to the junction. Therefore, one obvious improvement would be to implant through a thin SiO_2 layer to bring the concentration peak to the surface. Also, since CW laser annealing does not result in significant dopant redistribution, the emitter could be molded to any desired profile using this technique. At present, we are trying these and other ideas to optimize the CW laser-annealing process for solar cell applications.

REFERENCES

1. Young, R.T., Wood, R.F., Narayan, J., White, C.W., and Christie, W.H., "Pulsed Laser Techniques for Solar Cell Processing," IEEE Trans. on Electron Devices ED-27, No. 4, pp. 807-815, 1980.

2. White, C.W., Narayan, J. and Young, R.T., "Laser Annealing of Ion-Implanted Semiconductors," Science 204, pp. 461-468, 1979.

3. Wang, J.C., Wood, R.F., and Pronko, P.P., "Theoretical Analysis of Thermal and Mass Transport in Ion-implanted Laser-Annealed Semiconductors," Appl. Phys. Lett. 33, pp. 455-458, 1978.

4. Gat, A., Gibbons, J.F., Magee, T.J., Perg, J., Deline, V.R., Williams P., and Evans, C.A., Jr., "Physical and Electrical Properties of Laser Annealed Ion Implanted Silicon," Appl. Phys. Lett. 32, pp. 276-278 1978.

5. Auston, D.H., Golovchenko, J.A., Smith, P.R., and Surko, C.M., "CW Argon Laser Annealing of Ion-Implanted Silicon," Appl. Phys. Lett. 33, pp. 539-541, 1978.

6. Johnson, N.M., Gold, R.B. and Gibbons, J.F., "Electronic Defect Levels in Self-Implanted CW Laser-Annealed Silicon," Appl. Phys. Lett. 34, pp. 704-706, 1979.

7. Kimerling, L.C., "Defect States in Electron-Bombarded Silicon: Capacitance Transient Analyses," Radiation Effects in Semiconductors 1976 (Inst. Phys. Conf. Ser. 31, Bristol, 1977), pp. 221-230.

8. Watkins, G. and Corbett, J.W., "Defects in Irradiated Silicon. I. Electron Spin Resonance of the Si-A Center," Phys. Rev. 121, pp. 1001-1014, 1961.

Table I.- PROCESS STEPS FOR HIGH-EFFICIENCY SOLAR CELLS USING LASER ANNEALING

1. Ion implantation (5 keV B or As)
2. "Quick" clean
    1. $H_2O_2 + H_2SO_4$
    2. $HNO_3 + H_2SO_4$
    3. $H_2O + HF$
3. Laser anneal (E_d = 1.2 J/cm^2 with ruby Q-switched laser, substrate at 400°C)
4. Back side gettering
    A. Laser pulse (2.2 - 2.5 J/cm^2 through rough ground glass)
    B. "Quick" clean (see 2)
    C. Heat at 1000°C for 1 h in oxygen atmosphere
5. Polish the back
6. Back-surface field
    A. Deposit 100 A (B, p-type; Sb, n-type)
    B. Laser anneal at 1.8 J/cm^2
7. Mask front and back to etch the edge
8. RCA clean
    1. 5-1-1 of H_2O - 30% H_2O_2 - 27% NH_4OH (80°C for 15 min)
    2. 6-1-1 of H_2O - 30% H_2O_2 - 37% HCl (80°C for 15 min)
    3. $H_2O + HF$
9. Put on contacts (Ti/Pd/Ag) sinter 500°C/2 min
10. AR coating Ta_2O_5 at 500°C substrate

TABLE II. - RESULTING SOLAR CELL PARAMETERS FOR STEPS IN TABLE I

Method of fabrication	V_{oc} (mV)	J_{sc} (mA/cm^2)	FF	(%)
o As implantation, laser annealing for emitter region No BSF No gettering (steps 1-3, 7-10)	565	35.2	0.76	15.1
o As implantation, laser annealing for emitter region BSF by laser-induced diffusion No gettering (steps 1-3, 6-10)	595	34.6	0.78	16.1
o As implantation, laser annealing for emitter region BSF by laser-induced diffusion Minority carrier diffusion length enhancement by laser gettering (100 μm → 400 μm)	605	35.1	0.78	16.6

TABLE III.- A COMPARISON OF SOLAR CELL PARAMETERS FOR CW LASER ANNEALING AND PULSED LASER ANNEALING

Laser annealing technique	As Implant energy (keV)	Dose (x 10^{15}/cm^2)	Substrate Temp. °C	FF (%)	V_{oc} (mV)	J_{sc} (mA/cm^2)	η (%)
Pulse	5	1	400	79	585	34.1	15.8
Pulse	5	2	400	78	587	34.2	15.7
Pulse	5	4	400	78	595	34.6	16.1
Pulse	25	2	400	77	550	34.7	14.7
CW	100	3	500	78	510	26.5	10.5
CW[1]	100	3	500	78	532	27.5	11.4

[1]These samples were subjected to a 700°C furnace anneal for 1 h.

TABLE IV.- THE PARAMETERS USED FOR THE CALCULATED QUANTUM EFFICIENCIES SHOWN IN FIG. 2

	a)	b)	c)
Junction depth (μm)	.18	.18	.18
Cell thickness (μm)	280	280	350
Depl. region thickness (μm)	.91	.91	.88
Emitter diff. length (μm)	.01	.01	1.01
Base diff. length (μm)	100	130	500
Emitter diff. const. (cm^2/sec)	1.4	1.4	1.7
Base diff. const. (cm^2/sec)	34.2	34.2	34.1
Emitter recomb. vel (cm/sec)	10^7	10^7	$2x10^5$
Base recomb. vel (cm/sec)	10^2	10^2	10^2
Emitter dopant conc.(/cm^3)	$1.5x10^{21}$	$1.5x10^{21}$	$1x10^{20}$
Base dopant conc. (/cm^3)	$1.4x10^{15}$	$1.4x10^{15}$	$1.5x10^{15}$

TABLE V.- TRAP CHARACTERIZATION OF TRAPS FOUND IN n-on-p CW LASER-ANNEALED DIODES

QUANTITY	E-1	H-1
1. Trap type	Minority	Majority
2. Activation energy (E,eV)	0.174 ± 0.001	$0.674 + 0.012$
3. Majority capture cross section (cm^2)	1.3×10^{-20} at 77 K	4.1×10^{-18}
4. Minority capture cross section (cm^2)	$> 3 \times 10^{-15}$ at 77 K	-
5. Concentrations ($x10^{13}/cm^3$)		
1. CW Laser Annealed	0.4 ± 0.1	1.7 ± 0.1
2. CW Laser Annealed + Pulse Laser Annealed	0.3 ± 0.1	1.7 ± 0.1
3. CW Laser Annealed + 700°C Furnace Anneal	< 0.02	0.05 ± 0.05

6. Both defect profiles were independent of distance from the junction for the region measured (1 to 4 m).

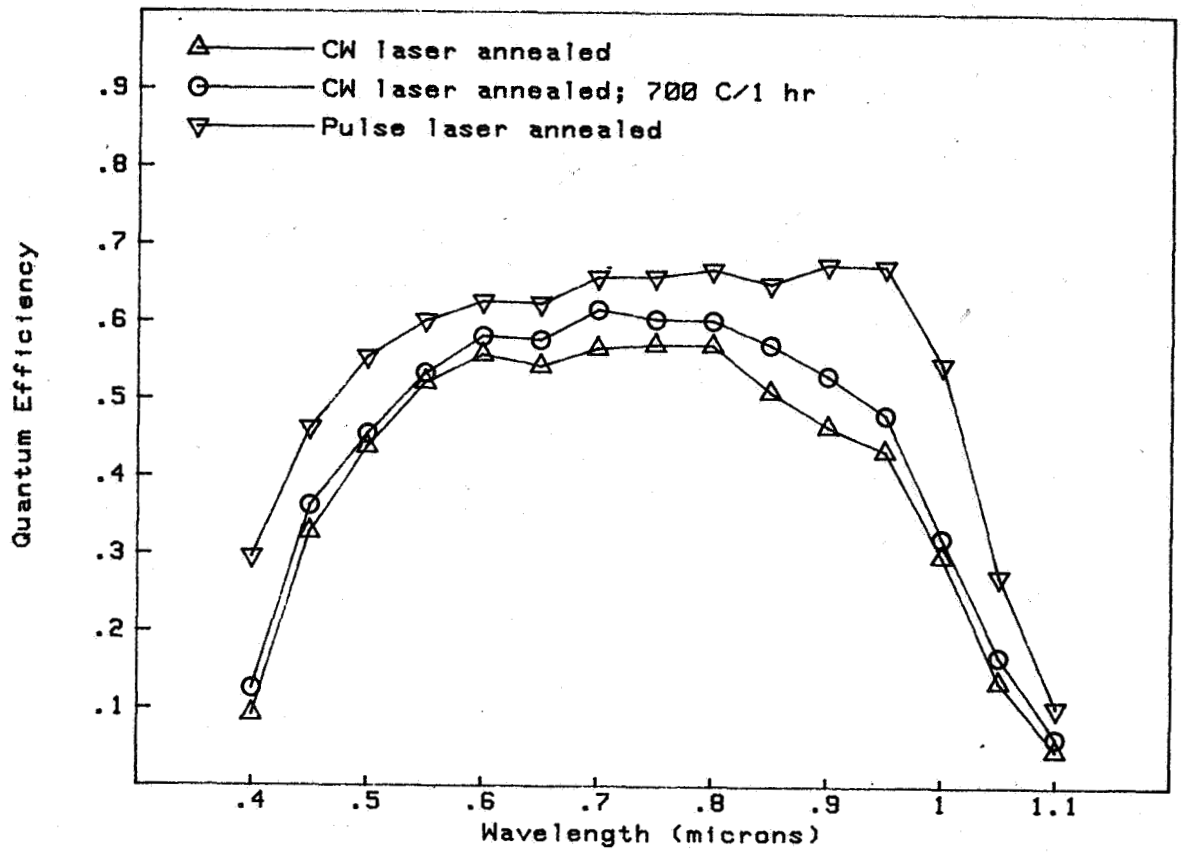

Fig. 1. Quantum efficiency measurements for solar cells without AR coatings fabricated using a) CW laser annealing, b) CW laser annealing plus 700°C furnace annneal for 1 h, and c) pulsed laser annealing.

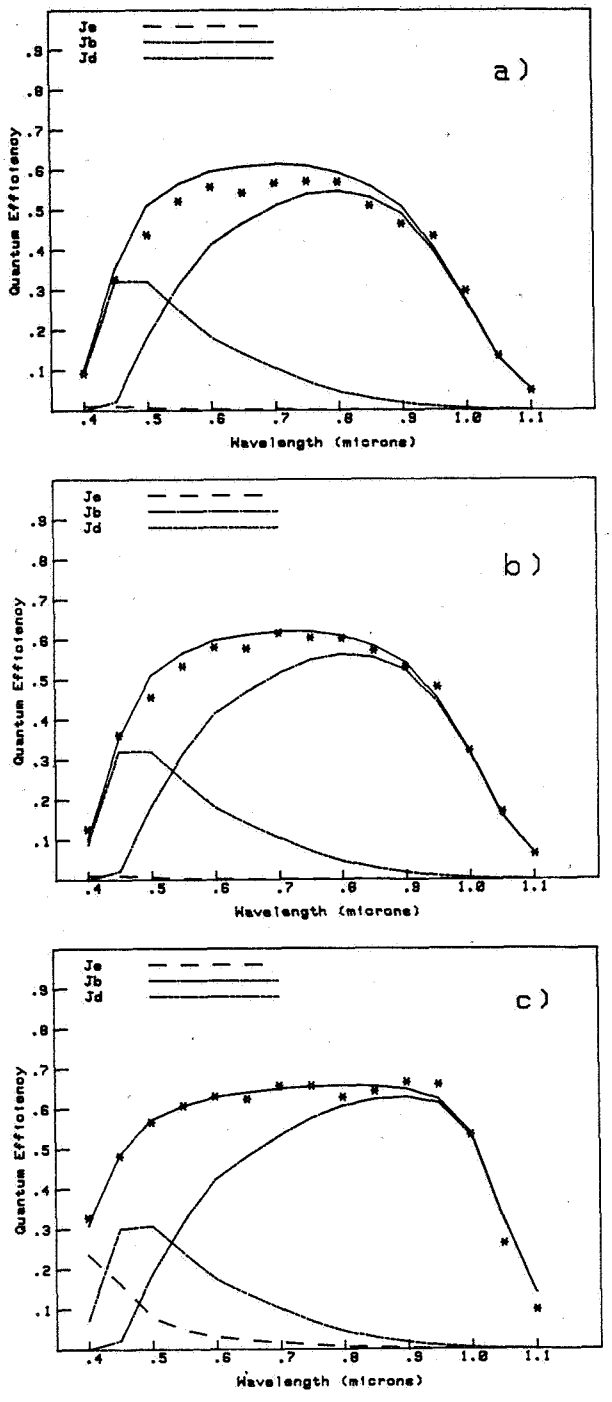

Fig. 2. Quantum efficiency measurements plus calculated quantum efficiencies showing total quantum efficiency (solid line), and the contributions from the emitter (Je, dashed line), the base (Jb, dashed-dotted line) and the depletion region (Jd, dashed double-dotted line). The cells are the same as those of Fig. 1, where a) is CW laser annealed, b) is CW laser annealed plus 700°C furnace anneal, and c) is pulsed laser annealed.

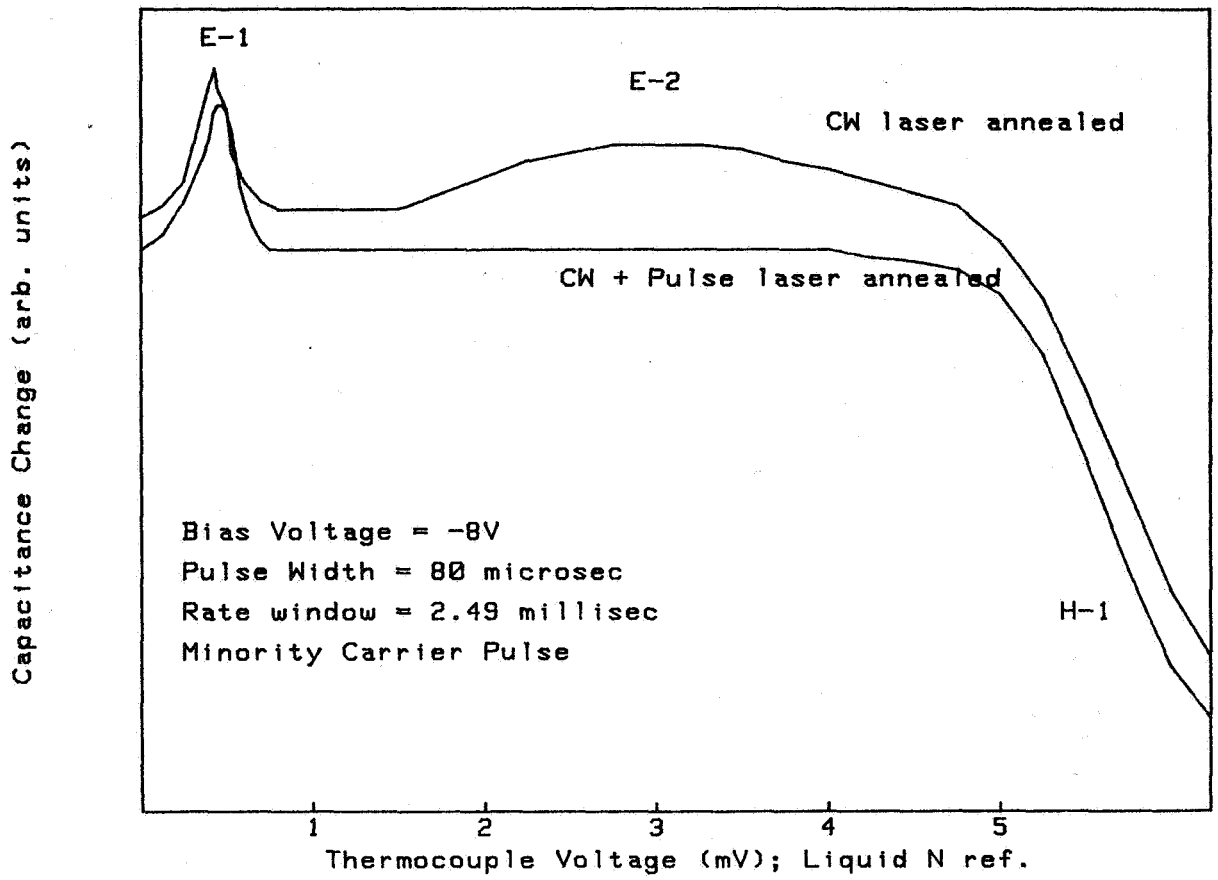

Fig. 3. DLTS spectra for diodes fabricated from 1) CW laser annealing and 2) CW laser annealing plus pulsed laser annealing.